

See discussions, stats, and author profiles for this publication at: <https://www.researchgate.net/publication/313358745>

# A Novel Anomaly Detection Approach to Identify Intentional AIS On-Off Switching

Article in *Expert Systems with Applications* · February 2017

DOI: 10.1016/j.eswa.2017.02.011

---

CITATIONS  
29

READS  
830

---

6 authors, including:



Fabio Mazzarella  
Luxottica  
21 PUBLICATIONS 371 CITATIONS

[SEE PROFILE](#)



Michele Vespe  
European Commission  
115 PUBLICATIONS 1,847 CITATIONS

[SEE PROFILE](#)



Alfredo Alessandrini  
European Commission  
37 PUBLICATIONS 1,128 CITATIONS

[SEE PROFILE](#)



Giuseppe Aulicino  
Coast Guard  
6 PUBLICATIONS 82 CITATIONS

[SEE PROFILE](#)

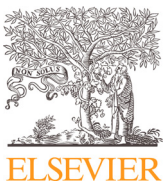
Some of the authors of this publication are also working on these related projects:



Flying radar [View project](#)



Positioning [View project](#)



# A novel anomaly detection approach to identify intentional AIS on-off switching



Fabio Mazzarella<sup>a,\*</sup>, Michele Vespe<sup>a</sup>, Alfredo Alessandrini<sup>a</sup>, Dario Tarchi<sup>a</sup>, Giuseppe Aulicino<sup>b</sup>, Antonio Vollero<sup>b</sup>

<sup>a</sup> European Commission, Joint Research Centre (JRC), Directorate Space, Security & Migration, Demography, Migration & Governance Unit, Via Enrico Fermi 2749, 20127 Ispra (VA), Italy

<sup>b</sup> Italian Coast Guard Headquarters, Via dell'Arte 16, 00144 Rome, Italy

## ARTICLE INFO

### Article history:

Received 5 August 2016  
Revised 3 February 2017  
Accepted 4 February 2017  
Available online 4 February 2017

### Keywords:

Automatic Identification System (AIS)  
Maritime surveillance  
Maritime Situational Awareness  
Received Signal Strength Indicator  
Anomaly detection  
Knowledge-based systems

## ABSTRACT

The Automatic Identification System (AIS) is a ship reporting system based on messages broadcast by vessels carrying an AIS transponder. The recent increase of terrestrial networks and satellite constellations of receivers is making AIS one of the main sources of information for Maritime Situational Awareness activities. Nevertheless, AIS is subject to reliability and manipulation issues; indeed, the received reports can be unintentionally incorrect, jammed or deliberately spoofed. Moreover, the system can be switched off to cover illicit operations, causing the interruption of AIS reception. This paper addresses the problem of detecting whether a shortage of AIS messages represents an alerting situation or not, by exploiting the *Received Signal Strength Indicator* available at the AIS Base Stations (BS). In designing such an anomaly detector, the electromagnetic propagation conditions that characterize the channel between ship AIS transponders and BS have to be taken into consideration. The first part of this work is thus focused on the experimental investigation and characterisation of coverage patterns extracted from the real historical AIS data. In addition, the paper proposes an anomaly detection algorithm to identify intentional AIS on-off switching. The presented methodology is then illustrated and assessed on a real-world dataset.

© 2017 The Authors. Published by Elsevier Ltd.

This is an open access article under the CC BY license. (<http://creativecommons.org/licenses/by/4.0/>)

## 1. Introduction

The maritime domain can be considered essential to the world's economy as over 90% of global trade is carried by sea. It actually represents the most effective way to move goods around the world. Moreover, maritime environment also involves the transportation of human beings, with more than 400 million passengers embarking and disembarking in European ports every year (European Commission, 2009). As some vessels may be engaged in illegal, illicit or dangerous activities, maritime transport and port security has become a major concern. One of the main pillars of maritime safety and security is Maritime Situational Awareness (MSA) -the capability of understanding events, circumstances and activities within and impacting the maritime environment- which is aided by surveillance and tracking systems.

The Automatic Identification System (AIS) technology, a ship reporting system originally designed for collision avoidance, is becoming a cornerstone of MSA. Ships of 300 gross tons and upwards in international voyages, 500 tons and upwards for cargoes not in international waters and passenger vessels are obliged to be fitted with AIS equipment (SOLAS, 2000). In addition, all the EU fishing vessels of overall length exceeding 15 m are also required to be fitted with AIS from May 2014 (European Parliament, 2002). Differently than other operational coastal active systems for maritime surveillance, AIS is characterized by considerable coverage (VHF propagation) together with a relatively accurate positioning performance (Angrisano, Gaglione, & Gioia, 2013). Moreover, the continuous increase of terrestrial networks and satellite constellation of receivers is providing global tracking data well-suited to be used in a wide range of applications beyond collision avoidance. Example applications include vessel tracking (Mazzarella et al., 2013; Mazzarella, Arguedas, & Vespe, 2015; Pallotta, Horn, Braca, & Bryan, 2014), extraction of knowledge (Pallotta, Vespe, & Bryan, 2013), vessel behaviour identification (Mazzarella, Vespe, Damalas, & Osio, 2014; Natale, Gibin, Alessandrini, Vespe, & Paulrud, 2015; Vespe et al., 2016), anomaly

\* Corresponding author.

E-mail addresses: fabio.mazzarella@jrc.ec.europa.eu (F. Mazzarella), michele.vespe@jrc.ec.europa.eu (M. Vespe), alfredo.alessandrini@jrc.ec.europa.eu (A. Alessandrini), dario.tarchi@jrc.ec.europa.eu (D. Tarchi), giuseppe.aulicino@mit.gov.it (G. Aulicino), antonio.vollero@mit.gov.it (A. Vollero).

detection on vessel movements (Handayani, Sediono, & Shah, 2013; Laxhammar, Falkman, & Sviestins, 2009; Ristic, La Scala, Morelande, & Gordon, 2008).

Given that the AIS is a self-reporting system, the main drawbacks of this technology are its reliability and susceptibility to manipulation. Therefore, the verification of the trustworthiness of AIS data is becoming a key problem to exploit the full potential of this technology not only for safety but for security applications as well. In this context, the main issues to be addressed are the following (Balduzzi, Pasta, & Wilhoit, 2014; Harati-Mokhtari, Wall, Brooks, & Wang, 2007): (i) AIS messages can be erroneous, because a part of the information is entered manually by the crew, both at the initialisation of the system for permanent data (e.g. the name of the vessel) and at every new journey for journey-related data (e.g. the vessel destination); (ii) AIS reports can be falsified (or spoofed) as a deceptive behaviour; (iii) a vessel can turn off its AIS transponder potentially to engage in illegal activities. The study in Iphar, Napoli, and Ray (2015) aims at pointing out the vessels for which AIS information are false or falsified, by using a methodology based on integrity and quality assessment of the AIS messages. Detection of AIS position spoofing has been studied in Papi et al. (2015), where the authors combine a classic radio-location method based on Time Difference Of Arrival (TDOA) with an Extended Kalman Filter designed to track vessels in geodetic coordinates. The authors in Katsilieris, Braca, and Coraluppi (2013) address instead the inference problem of whether the received AIS data are trustworthy with the help of radar measurements. Up to the authors' knowledge, the work by Guerriero, Coraluppi, Carthel, and Willett (2010) is the only one in literature addressing the detection of the AIS status (on/off). In particular, the AIS intermittency has been there analysed using the mathematical formalism of Hidden Markov Models (HMM) and the characteristics of the AIS transmission channel have been taken into consideration.

This paper is devoted to the analysis of AIS data for the purpose of detecting whether the absence of AIS measurements is representative of an anomalous event (e.g. intentional on-off switching), or it can be ascribed to a channel communication dropout. The emission termination detection, as already described in Guerriero et al. (2010) is a challenging problem due to the high level of fluctuations in the AIS signal, meaning that the probability of receiving a transmitted AIS message can undergo significant variations.

The main contribution of this paper is twofold. The focus of the first part is on a comprehensive experimental investigation of open sea radio wave propagation of the AIS messages, deepening the preliminary study in Mazzarella, Vespe, Tarchi, Aulicino, and Vollero (2016). Such an analysis is based on the Received Signal Strength Indicator (RSSI), a feature available at receivers, and rarely exploited in the wide range of applications in the maritime domain. This study, that at our knowledge is not available in literature for this kind of systems, is essential to build the sound models suitable to be used within the proposed architecture aimed at detecting suspicious lack of AIS messages. Second, we propose a general approach for the detection of anomalous AIS dropouts. The main work in literature dealing with the AIS messages dropouts detection is the one in Guerriero et al. (2010), where only the AIS reports presence/absence information is taken into account. The architecture proposed in this paper exploits an additional feature, the RSSI, in order to improve the detection capabilities. In addition, the detector can be operated both in off-line and on-line scenarios. Many surveillance applications present indeed a strong limitation because they are based on the assumption that anomaly classification is performed after the whole trajectory has been observed and this delays the detection of alerting events.

The paper is organized as follows. Section 2 provides a general overview of the proposed methodology and emphasize the need of a thorough analysis of the AIS coverage patterns. The characterisa-

tion of the AIS reception behaviour is developed in Section 3. In Section 4 the anomaly detection algorithm is discussed, together with the analysis of features used for the experimentation. The proposed algorithm is applied to real-word data and the performance is evaluated in Section 5, while conclusions are reported in Section 6.

## 2. Methodology

While analysing the AIS records, the events of interest, as described in Guerriero et al. (2010), are the reception of new messages and the dropout, namely the loss of AIS messages. In particular, a dropout can occur whenever the AIS transponder correctly broadcasts the message, but it is not received by the BS because of the communication channel-related effects (vessel range out of Line-Of-Sight (LOS), fading, multipath, shadowing). Nevertheless, a dropout can be the effect of an intentional transmission termination to cover illicit activities. The main goal of this paper is the automatic discrimination between channel-related dropouts and intentional ones. The detection of such events is challenging mainly for two reasons. First of all, because of the irregular nature of AIS data whose reporting interval changes from few seconds to several minutes. Second, the radio wave propagation phenomena for an open and congested environment like the sea are very structured and greatly affect the behaviour of the RSSI at the BS. The flowchart of the proposed methodology is summarized in Fig. 1 for a single receiving BS.

Anomaly detectors generally compare test events against pre-built normality models, in order to classify them as anomalous or regular. The core of the architecture is thus represented by two normality models, as highlighted in Fig. 1 by the two yellow rectangles. On the one side, the historical AIS data received by a single BS in a certain time interval are used as a training data set to build a data-driven normality model for the BS. As it will be discussed throughout the paper, this can be achieved by exploiting the RSSI, the vessel positions and their corresponding distances from the BS as model features, and standard tools from machine learning. On the other side, the single vessel normality model is based on the theoretical aspects affecting the electromagnetic propagation between the BS and the vessel antenna. These phenomena are strictly dependent on vessel-related features, like the height of the transmitting antenna.

From an operational point of view, let's pretend to gather a test vessel track, that is generally the output of a tracking system. By following the workflow in Fig. 1, the test track is periodically analysed to look for potential dropouts. If an AIS message dropout occurs at a certain time  $t_d$ , the following steps take place. First, features have to be extracted from the vessel track in order to make a comparison to the normality models. Accordingly, an estimation (or a prediction) of the vessel position at the dropout time  $t_d$  can be obtained from the tracking system and, consequently, an estimation of the distance between the BS and the expected vessel position is available. The reconstruction of the RSSI missing value is obtained, instead, through the *imputation* step in Fig. 1. Although missing data is not a well-studied area in the maritime domain, many missing data imputation methods have been developed outside of the maritime domain research area, including Nearest Neighbors imputation (NN) (Jiahua Chen, 2001; Rancourt, 1999), Bayesian-based imputation (Hruschka, Hruschka, & Ebecken, 2007), and regression-based imputation (Fox, 2008). Once the missing message has been reconstructed, it can be compared to the normality models in order to obtain two scores, one from the BS normality model and the other one from the single vessel model, revealing the likelihoods of the imputed message over the normality models. A joint statistics obtained by combining the single likelihoods will be compared to a threshold in order to flag

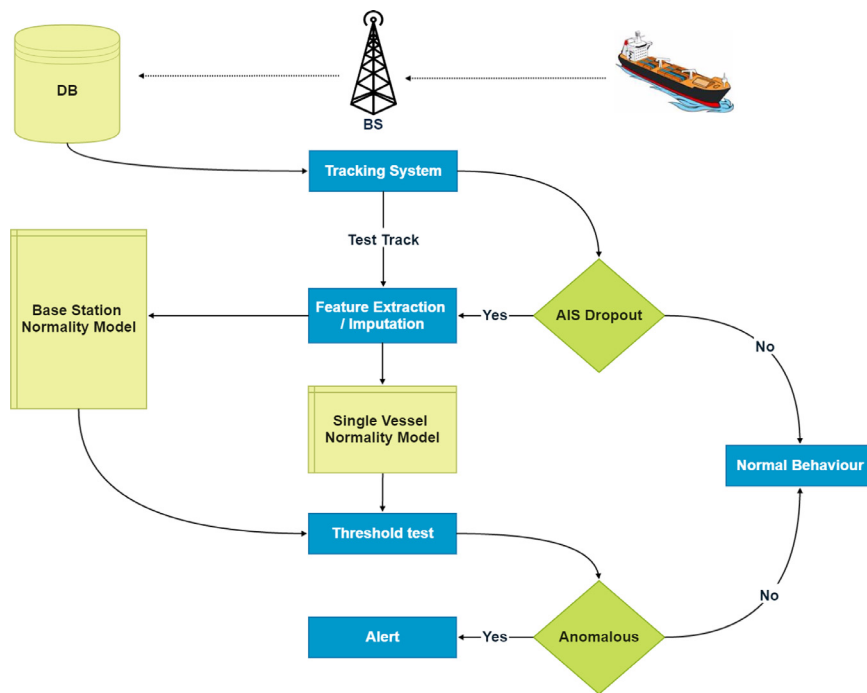


**Fig. 1.** General flowchart of the AIS on/off detection approach.

the dropout as anomalous or regular. In particular, if the decisions statistics is greater than a defined threshold, a decision in favour of the anomalous behaviour will be made.

### 3. AIS reception characterisation

In order to better understand the impact of the various VHF propagation effects on AIS transmission, it is necessary to give a brief review of the fundamentals of AIS technology. The transmission frequencies, powers and antenna gains are all important considerations when analysing the propagation phenomena illustrated in this work.

AIS was born as a collision avoidance system and is based on regular VHF transmission and reception of binary messages containing information about the vessel dynamic state (e.g. position, Speed Over Ground (SOG), Course Over Ground (COG), Rate Of Turning (ROT)) and static/voyage-related information (e.g. MMSI number, name, call sign, destination, vessel type, size) of ships. This set of observations can be linked to other information available at each terrestrial BS (Time Of Arrival (TOA), RSSI, Signal to Noise Ratio (SNR)). Dynamic data reporting rates change with vessel speed from a minimum of 2 s at speed greater than 23 knots to 3 min for ships at anchor. For the static part, a report is broadcast every 6 min. The two VHF operating bands are  $f_1 = 161.975$  MHz and  $f_2 = 162.025$  MHz. The standard AIS devices are known as *Class A* AIS and they must operate continuously. In 2007, *Class B* was introduced for small craft, including pleasure vessel. In the remainder of the paper, we will focus on *Class A* systems only.

#### 3.1. AIS path loss propagation

Being AIS conceived as a collision avoidance system, it needed only a LOS communication system and therefore the VHF band of frequencies was ideal for terrestrial use. This often limits the range to about 40 nautical miles but it can be greater under favourable propagation conditions. The typical range in kilometres,  $R$ , can be

estimated from  $h_T$  and  $h_R$ , the heights of the antennas in transmission and reception, respectively, by using the approximation in [Barclay \(2003\)](#)

$$R \approx 4.131(\sqrt{h_T} + \sqrt{h_R}), \quad (1)$$

where it is assumed that the troposphere has its average properties, corresponding to setting the radius of the earth to 4/3 of its true value.

While analysing the maritime communication in the open sea environment, the LOS and reflections from sea surface are considered the relevant components of the RSSI, while reflections from shore and noise are considered as undesired components which need to be removed. However, a number of phenomena produce interference signals with the effect of extending the signal range beyond the LOS. In the literature dealing with the electromagnetic propagation in the VHF band, three main phenomena were determined to have a tangible effect on the AIS transmission.

- Diffraction over the sea around the curvature of the earth should be taken into account because it extends the range of the AIS signals.
- Multipath effects can produce variability in the RSSI and strongly depends on how a transmitting ship antenna is mounted, the ship superstructure, the wind speed, and the receiver configuration, including the height of the antenna and surrounding terrain.
- Ducting, occurring when the vertical gradient of the refractivity profile of the troposphere is greater than a certain threshold, can also extend the transmission range.

Other phenomena, like as tropospheric scatter and scattering linked to the ionospheric layers, do not have a considerable effect on the extension of the AIS transmission range ([Green, Fowler, Power, & Tunaley, 2011](#)).

The simplest approach for predicting the propagation characteristics of radio waves is to employ ray theory, that is based on the geometric optics model. In free space the waves propagate in straight lines within ray tubes. In addition, the well-known

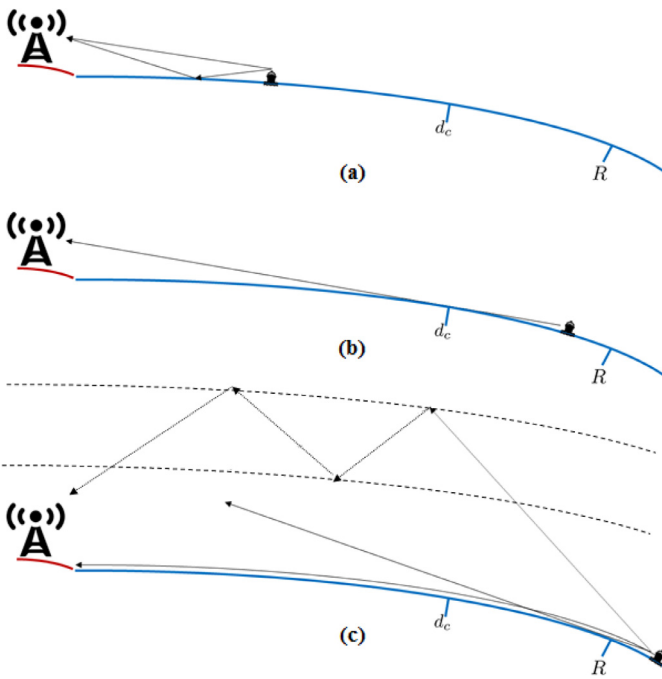


**Fig. 2.** (a) LOS PEL region. Within this region, before the critical distance, the PEL approximation can be considered accurate and the received signal is mainly made of the LOS and sea-reflected rays. (b) LOS REL region. In between critical distance and LOS range, the curvature of the earth starts shadowing the LOS ray and a REL model should be adopted. (c) Over The Horizon (OTH) propagation. In this region, LOS and sea-reflected components cannot reach the receiving antenna, but ground-wave propagation and tropospheric ducting effect make signal reception possible also in this range.

link budget allows for accounting gains and losses occurring between the transmitter and the receiver through the communication medium. In the following, it is shown how the link budget can be made more complex in order to take into consideration much more non-ideal phenomena.

In general, we can summarize the relationships between the transmitter and the receiver powers through the following equation:

$$\begin{aligned} P_R &= \frac{P_T G_T G_R}{L_{FS} L_T L_R L_M}, \\ &= \frac{P_T G_T G_R}{L}, \end{aligned} \quad (2)$$

where  $P_R$  and  $P_T$  are the received and transmitted powers,  $G_T$  and  $G_R$  are the antenna gains in transmission and reception, respectively,  $\lambda$  is the wavelength and the term  $L$  takes into account the path loss ( $L_{FS}$ ), receiver losses ( $L_R$ ), transmitter losses ( $L_T$ ), and miscellaneous losses ( $L_M$ ) due to multi-path fading effects, shadowing and atmospheric propagation losses.

In the simplest case and considering only the LOS component of the received ray, the power  $P_R$ , received from a Class A transmitter at an unobstructed range  $d$  is given by the well-known Friis equation:

$$\begin{aligned} P_R &= \frac{P_T G_T G_R}{L_{FS}} \\ &= P_T G_T G_R \left( \frac{\lambda}{4\pi d} \right)^2. \end{aligned} \quad (3)$$

When a reflected ray from the sea surface exists beside the LOS path, as depicted in Fig. 2(a), the propagation loss could be predicted by a two-ray path loss model, that under the assumption

of Plan Earth (PEL) (Yang, Ekman, Rste, & Bekkadal, 2011) can be approximated as

$$L_{2-ray}^{PEL} = \left( \frac{\lambda}{4\pi d} \right)^2 \left| 1 + \rho \exp \left( jk \frac{2h_R h_T}{d} \right) \right|^2, \quad (4)$$

where  $k$  represents the wave number and  $\rho$  is the reflection coefficient from sea surface. This model considers constructive and destructive interference phenomena occurring when the LOS and the reflected rays are in phase and out of phase respectively.

For distances beyond several kilometres, when the scenario is the one displayed in Fig. 2(b), the earth cannot be considered plane and a round earth geometrical model should be taken into consideration. In particular, the model in (4) is quite accurate roughly up a critical distance  $d_c$  that can be estimated as

$$d_c = \frac{4h_T h_R}{\lambda}. \quad (5)$$

For distances greater than  $d_c$  a Round Earth Model (REL), as described in Yang, Molisch, Ekman, and Roste (2013), should be adopted. In this case, the path loss can be approximated as

$$L_{2-ray}^{REL} = \left( \frac{\lambda}{4\pi D_{LOS}} \right)^2 |1 + \rho \exp(jk D_{diff})|^2. \quad (6)$$

Here,  $D_{LOS}$  represents the path length of the LOS,  $D_{diff}$  is the path length difference between the LOS and sea reflection. Further details on this model can be found in Yang et al. (2013). However, the round earth geometrical model only takes the sea reflection into consideration, based on the two-ray method. This is not enough because the earth curvature will gradually shadow both the LOS and the sea reflection as the transmitter/receiver distance increases. In addition, divergence on the reflection path from the spherical earth curvature need to be taken into account. Last but not least, the effective reflection coefficient from the rough sea surface is also different from that of idealized specular reflections.

The earth curvature will not only block the reflected ray but also the LOS. However, the diffraction effect will allow the radio transmission to continue even beyond the LOS, though suffering from a diffraction loss. Several papers (Bullington, 1947; Norton, 1941) show the theory of ground-wave propagation over a smooth spherical earth, which fits the geometrical environments of the open-sea. A further refinement of the estimated propagation loss can be achieved by using a multi-ray path loss model taking into considerations other phenomena, like the ducting effects occurring when there are significant temperature increases at high altitudes and can allow for the reception of AIS signals even from vessels that are up to 1000 km away from the receiver. The propagation phenomena over the LOS are depicted in Fig. 2(c).

The International Telecommunications Union (ITU) has provided in ITU (2013) a procedure to be adopted for point-to-area prediction of field strength for the broadcasting, land mobile, maritime mobile in the frequency range 30 MHz to 3000 MHz. In particular, the recommendation provides a set of propagation curves of measured field-strength values for 1 kW effective radiated power at nominal frequencies of 100, 600, and 2000 MHz, respectively. The curves are based on measurements data mainly related to mean climatic conditions in temperate regions. In addition, the documentation in ITU (2013) proposes an algorithm in order to obtain the field strength from the provided measurements for a desired set of input parameters (e.g. transmitter power, distance, heights of antennas, etc...)

### 3.2. Single vessel analysis

In the following, in order to acquire an understanding of the AIS propagation behaviour and compare raw messages to the models

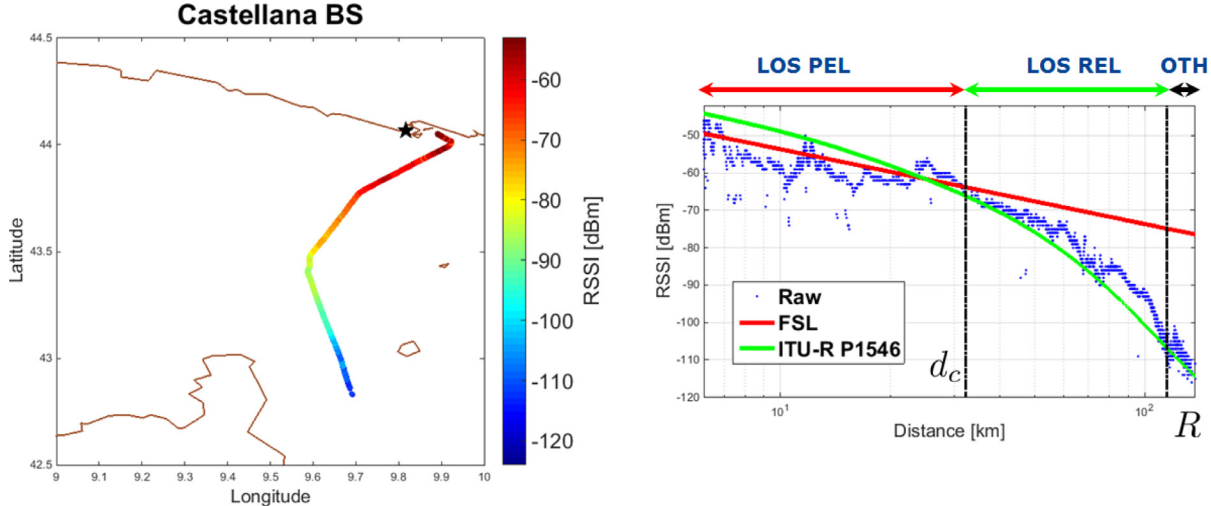


**Fig. 3.** Received Signal Strength Indicator (RSSI) from the BS located in Castellana, Italy, in the Ligurian Sea, for an oil/chemical tanker tracked between March 10 and 11, 2016. The left plot shows the track with both positional and power information. On the right plot, the behaviour of the RSSI is depicted versus the distance between the BS and the vessel. Blue dots refer to raw data, red line represents the Free Space Loss (FSL) model approximation, and the green curve is based on the ITU-R model in [ITU \(2013\)](#). In addition, the left black dashed line refers to the critical distance,  $d_c \approx 32$  km, while the right black dashed line refers to the LOS range,  $R \approx 115$  km. Deep fadings at  $d \approx 10$  km and  $d \approx 16$  km are due to multipath phenomena, when LOS and sea reflection are out-of-phase. (For interpretation of the references to colour in this figure legend, the reader is referred to the web version of this article.)

discussed in [Section 3.1](#), we will present and analyse real AIS data collected by a single BS for single vessels. In particular, we have referred to the Italian AIS network, that has been completely upgraded in 2012–2013 and consists of 60 BS mainly located to get the best VHF coverage (up to 100 nmi, even without the duct effect).

The left plot of [Fig. 3](#) displays the trajectory associated to AIS messages broadcast from an oil/chemical tanker to the BS located in La Spezia, on the Ligurian Sea, where the colourbar refers to the RSSI at the BS for each received AIS message. The plot on the right, instead, shows the behaviour of the RSSI versus the distance between vessel and BS, in semi-logarithmic scale, as the ship approaches the port of La Spezia. In particular, blue dots represent raw data as it is measured at the BS, the red line is the FSL approximation in [\(3\)](#), and the green curve is the model provided in [ITU \(2013\)](#). The vessel under investigation belongs to the class of large ships, with a length of 183 m and width of 27 m and approximated height of the AIS antenna  $h_T \approx 30$  m. The BS is mounted on the Monte Castellana and the height of the receiving antenna is  $h_R \approx 500$  m. By using these values in [\(1\)](#), we get a LOS distance of  $R \approx 115$  km, represented by the right black dashed line in [Fig. 3](#). Indeed, [Fig. 3](#) confirms that the BS starts receiving messages from the ships when its distance is around 120 km. The red line in [Fig. 3](#) has been obtained by considering for both antennas a gain  $G_T = G_R = 2$  dBi, as suggested in [Green et al. \(2011\)](#), while the power of transmitter is  $P_T = 12.5$  W as defined by the AIS standard. The right plot in [Fig. 3](#) reveals the very fluctuating nature of the RSSI signal and presence of several fading effects. Deep fadings with very short duration can be mainly attributed to other passing ships blocking the radio link between the BS and the vessel under analysis. Deep fadings with longer duration, like the ones in [Fig. 3](#) at  $d \approx 10$  km and  $d \approx 16$  km are due to multipath, when the path length difference between LOS and the sea reflection is a multiple of half wavelength and the two rays are out-of-phase. However, it is clear that the FSL-like behaviour is followed around the range 0–40 km. In particular, the FSL model is able to predict the exponential decreasing strength trend for the receiver under analysis and it is well-suited for the prediction of the local mean propagation loss. Approximation [\(5\)](#) sets indeed the critical

distance to  $d_c = 32.2$  km and it is represented by the left dashed black line in [Fig. 3](#). Beyond this distance, the phenomena linked to the curvature of the earth discussed in [Section 3.1](#) will make the FSL model invalid. In this region, at least the two-ray model based on the REL approximation [\(6\)](#) should be used, as described in [Yang et al. \(2013\)](#). However, the green curve in [Fig. 3](#) fits the measurements results between the critical distance and the LOS range, while does not perfectly match the raw data for short distances.

The scenario depicted in [Fig. 4](#) is the same of the one in [Fig. 3](#) but for a different vessel and a different time interval. In this case, the vessel tracked is a container ship approaching the port of La Spezia. The vessel size is greater than the oil/chemical tanker considered in the above, with a length of 303 m and a width of 40 m. We consider the height of the transmitter  $h_T \approx 50$  m, with a LOS range approximation of  $R \approx 121$  km as confirmed by the green dashed line on the right plot in [Fig. 4](#). Because of the greater height  $h_T$ , the FSL model is followed longer until the critical distance of  $d_c = 53$  km, represented by the black dashed line in [Fig. 4](#). Also in this case, the ITU-R model well approximate the behaviour of the RSSI between the critical distance and the LOS range. In addition, in this particular scenario, a reception is available also for distances greater than the LOS range.

The scenarios just discussed are interesting because they show how the AIS propagation behaviour changes, for the same geographic conditions and same receiver, as the vessel and the atmospheric conditions change. This means that the building of a single vessel-based normality model is essential in designing an anomaly detector as the one in [Fig. 1](#). In addition, the outcomes of comparisons between real RSSI measurements and the models in [Section 3.1](#), drive us to adopt a quasi-deterministic single vessel normality model comprising of the FSL approximation when the distance between transmitter and receiver is less than the critical distance and the ITU-R P.1546 model for distances until to the LOS range. The single vessel normality model is thus built on the theoretical and empirical aspects that rule the path-loss propagation for the open sea environment. The features that play a key role in building the model are the distance between vessel and BS, and the heights of the antennas.

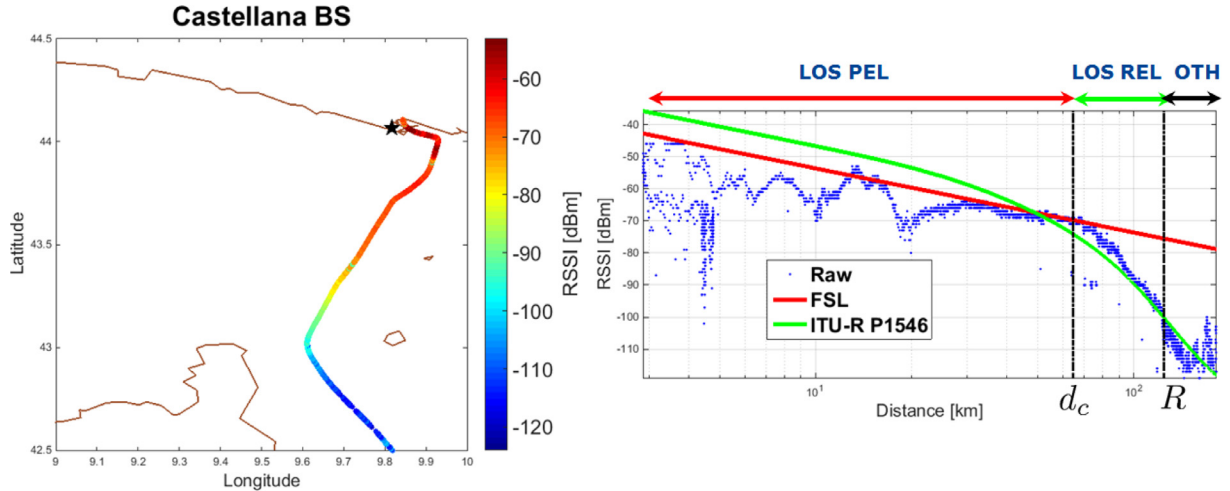


**Fig. 4.** Received Signal Strength Indicator (RSSI) from the BS located in Castellana, Italy, in the Ligurian Sea, for a container ship tracked between February 2 and 3, 2016. The left plot shows the track with both positional and power information. On the right plot, the behaviour of the RSSI is depicted versus the distance between the BS and the vessel. Blue dots refer to raw data, red line represents the Free Space Loss (FSL) model approximation, and the green curve is based on the ITU-R model in ITU (2013). In addition, the left black dashed line refers to the critical distance,  $d_c \approx 53$  km, while the right black dashed line refers to the LOS range,  $R \approx 121$  km. Very clear deep fadings at points  $d \approx 6$  km,  $d \approx 10$  km and  $d \approx 18$  km are due to multipath phenomena, when LOS and sea reflection are out-of-phase. (For interpretation of the references to colour in this figure legend, the reader is referred to the web version of this article.)

### 3.3. Base station behaviour

The general architecture proposed in Fig. 1 for the detection of anomalous AIS message dropouts, requires the building of a normality model for the BS under investigation. In order to understand the phenomena affecting the relationships existing amongst the relevant variables, we analyse the behaviour of the whole aggregate information coming from the ships seen by a certain BS in a certain time interval.

In general, the propagation phenomena linking the transmitter and receiver within the LOS range, can be summarized as in (2). As already mentioned in Section 3.2, the term  $L$  takes into account receiver loss (this part can be assumed constant for all stations), transmitter loss (this is averaged out by considering multiple vessels), fading effects due to multipath, shadowing and atmospheric propagation losses. While analysing the aggregate behaviour of all messages received by a BS, multipath is also averaged out given the variable antenna height between different ships that results in constructive/destructive interferences at different distances from the receiver. On the contrary, atmospheric attenuation involves mainly atmospheric scattering (very low absorption at VHF) and is quite dependent on meteorological conditions, therefore it varies geographically and with time. The effect of shadowing also is geographically variable and depends on events like temporary occlusions due to other ships along the LOS, or due to the orography around the receiver, therefore more stable with respect to time. The analysis of the RSSI data collected for all the vessels seen in a certain time interval is thus supposed to provide evidences on the features necessary to the building of a data-driven normality model for a single BS.

It is worth noting that the presence of mountains surrounding the AIS base station can make possible the indirect reception of messages beyond LOS due to reflections. Non-LOS propagation can also help in specific atmospheric conditions thanks to surface wave scattering and tropospheric ducting propagation. This effect happens when there are significant temperature increases at high altitudes and can allow for the reception of AIS signals even from vessels that are up to 1000 km away from the receiver.

The patterns depicted in Fig. 5(a)–(d) show the Class A-equipped ships traffic together with the information on the RSSI

measurements collected by several BS in the same time interval, between February 1st and February 7th, 2016. As already mentioned, being the traffic made of a great number of ships, we expect the RSSI behaviour for each BS to be uncorrelated on the transmitter features (e.g. antenna gain, transmitting power, multipath phenomena). From (2) we can state that, within the LOS range, given a certain distance  $d^*$ , the average receiver power  $P_R$  values should be comparable amongst all the BS. For a desired BS, the *radio horizon* is defined in (1) and the actual service range of the BS under normal weather conditions is approximated as

$$R \approx 4.131\sqrt{h_R} \quad (7)$$

However, on one hand Fig. 5(a)–(d) shows that RSSI dynamics are comparable and most of the received power is contained within the service range, depicted by the red circles, according the approximation in (7). On the other hand, they prove that a certain degree of asymmetry exist between different stations. For instance, the BS in Gorgona (Fig. 5(b)) shows a greater coverage towards open sea than in the other directions; the BS on Elba Island (Fig. 5(d)) has a low coverage in the South-East direction; and the BS in Pantelleria (Fig. 5(a)) shows unexpected behaviour towards South. These differences arise because the BS radio wave coverage is strongly dependent on the antenna radiation pattern and therefore orientation, and the sites where the antennas are mounted and that often are not in favourable positions.

The plots in Fig. 6 represents, instead, the behaviour of the RSSI collected by the Pantelleria BS by considering three different vessel classes based on their lengths. The plots depicted in Fig. 6 highlight the fact that the length of vessel affects the behaviour of a BS, because this dimension is strictly linked to the height of the transmitting antenna. This can be seen from top left plot of Fig. 6, where the extension of the radio coverage is reduced with the respect to the other plots. In summary, while building a normality base for a BS, it is fundamental to construct different models based on the vessel size, in order to reduce the false alarm probability of the anomaly detection algorithm.

As already stated, the AIS radio coverage can go beyond the LOS distance because of several phenomena. Fig. 7 shows indeed the behaviour of the Genoa BS for a time interval different from that

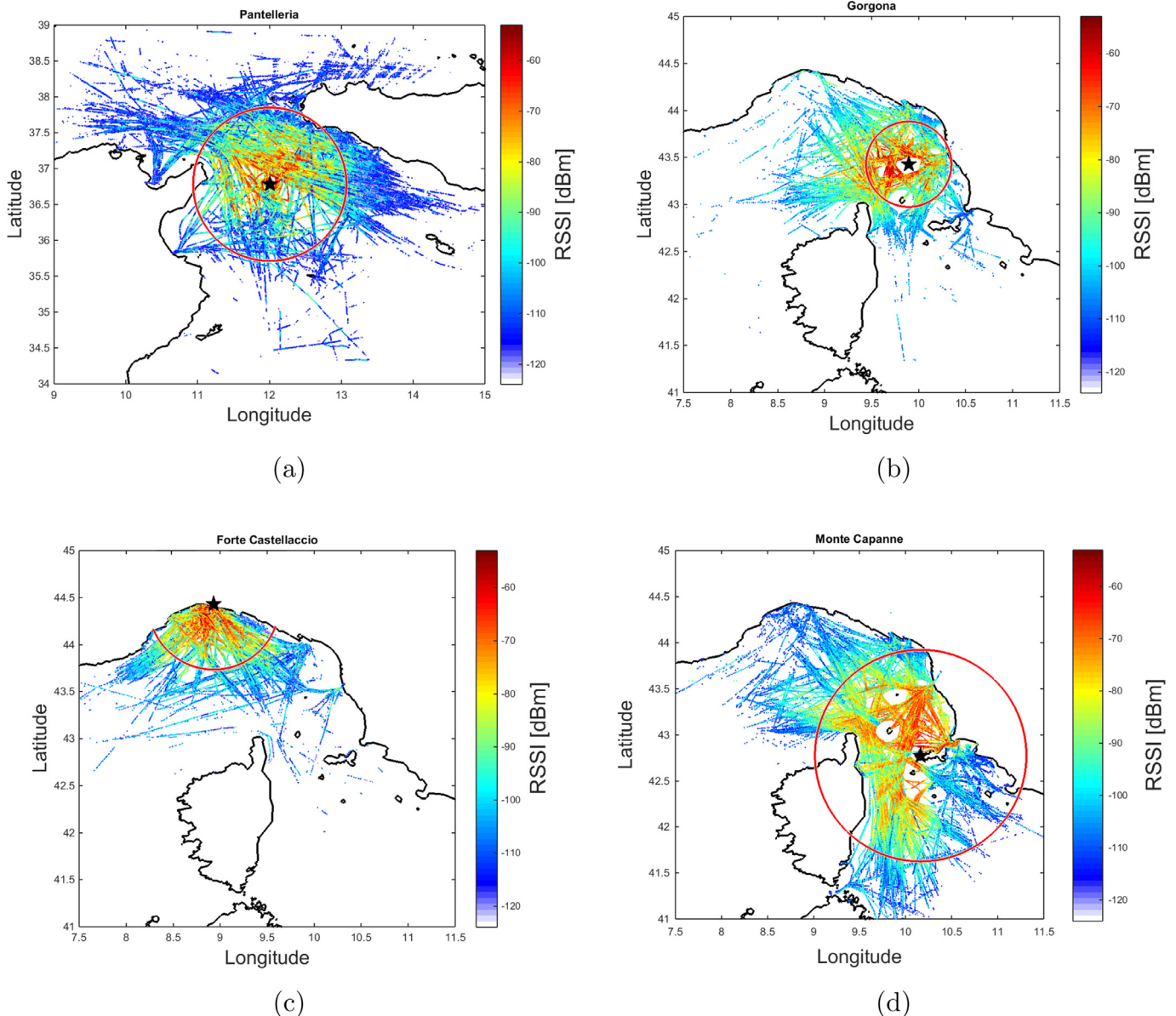


**Fig. 5.** Aggregate behaviour of the RSSI measurements collected by the (a) Pantelleria, (b) Gorgona Island, (c) Forte Castellaccio, Genoa, and (d) Monte Capanne on Elba Island Base Stations between February 1st and February 7th, 2016. Red circles represent the service ranges of the BS according to (7). (For interpretation of the references to colour in this figure legend, the reader is referred to the web version of this article.)

represented in Fig. 5(c). In particular, the theoretical LOS range approximated as in (7) is depicted by the red circle and it is less than 100 km. From the figure it is clear that the BS is able to receive messages much more farther than the LOS range and this is due to the tropospheric ducting affecting the area under analysis because of the hot temperatures during the month of July.

The scenarios analysed in this section, based on real-world measurements, show that a BS-based normality model should be built by taking into consideration several features of the available AIS messages: vessel geographical positions, RSSI and vessel sizes. As it will be clear later, this model can be obtained in a data-driven way, by exploiting historical AIS messages.

#### 4. The anomaly detection algorithm

The flowchart depicted in Fig. 1 consists of two main stages: the building of two normality models (one for the single vessel and another one for the BS behaviour) and the detection of inten-

tional AIS on-off switching events. During the first process, normal scenarios, i.e. anomalies-free, are taken into account and a representative background is created according to the considerations of Section 3. In the second step, instead, a decision is made by comparing the available observations to the normality models. The top panel of Fig. 8, obtained by broadening the flowchart in Fig. 1, depicts the block diagram of the normality models building stage. As for the single-vessel based normality template,  $\lambda_v$ , it is based on the theoretical/empirical considerations illustrated in Section 3.1. The BS normality model,  $\lambda_{BS}$ , instead, is built in a data-driven way, by exploiting historical AIS data. In particular, the training data set for the BS under consideration is conveniently pre-processed and a feature selection process aims at selecting those data characteristics useful to the creation of a background normality model. As it will be discussed later, two different approaches have been exploited to build the model of the BS normality behaviour: the *One-class Support Vector Machine* (SVM) and the *Averaged RSSI Rasters* (ARR).

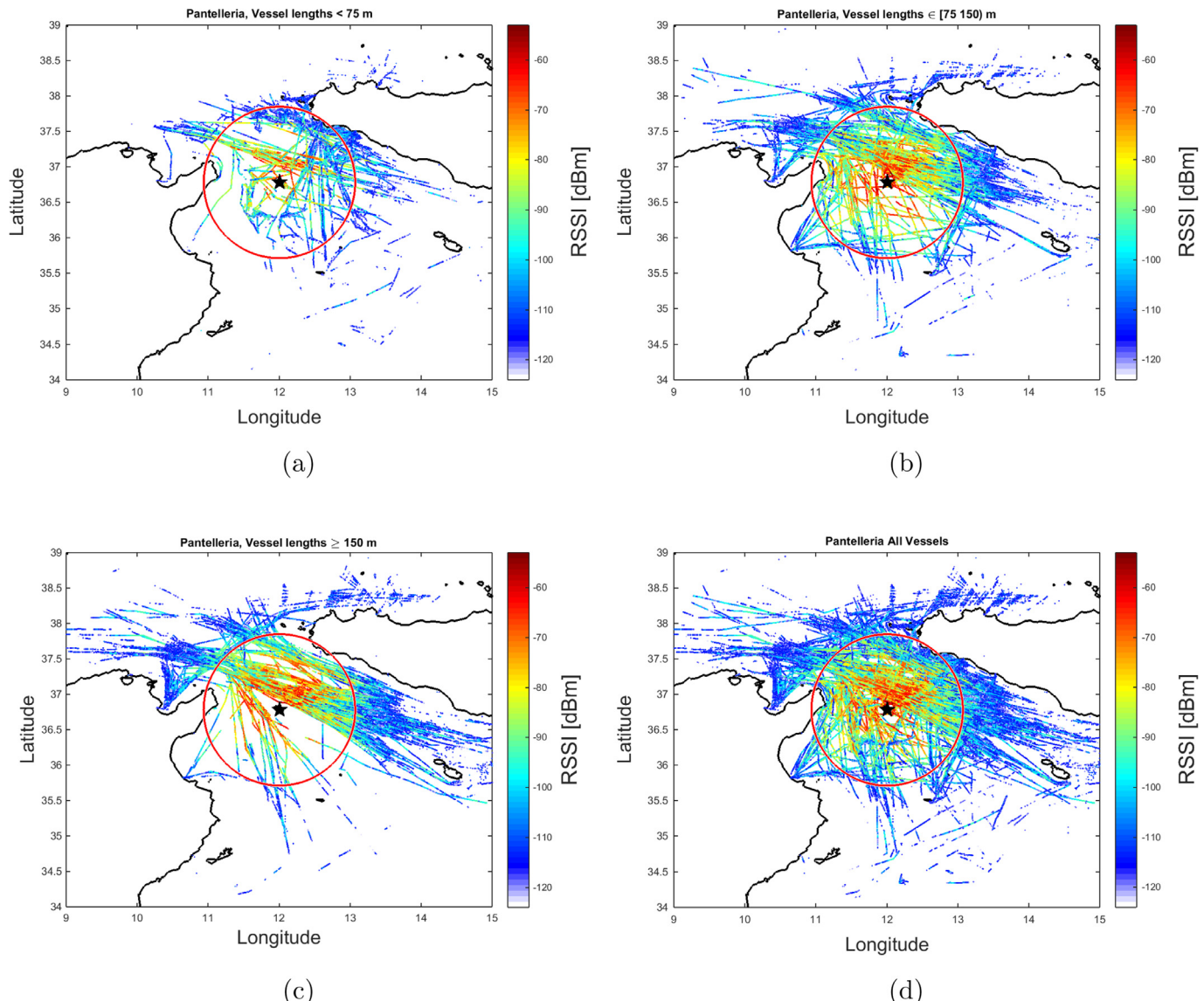


**Fig. 6.** RSSI measurements collected at the Pantelleria BS, for the following vessel size classes. From top left panel, clockwise: 1) vessel lengths  $< 75$  m; 2) vessel lengths in range  $[75, 150]$  m; 3) vessel lengths  $\geq 150$  m; 4) all vessel lengths.

In the second stage, represented in the bottom panel of Fig. 8, the feature extraction process is repeated on the test data set, for each vessel track that can contain anomalous events. Features extracted at this point are used to compute two risk levels, one,  $r_v$ , from the single vessel-based model, and another one,  $r_{BS}$ , from the BS-based normality model. They are then combined into a joint risk level,  $r$ . The comparison between the final risk level and a threshold,  $\epsilon$ , will provide a decision on the state of the nature, whenever a dropout occurs.

#### 4.1. Feature extraction

As described in Section 3, the features that can be considered essential to the building of the normality models are represented by the following information contained in both dynamic and voyage-related/static information of AIS messages available at the BS: (i) vessel position in latitude/longitude coordinates,  $x_{lon}$ ,  $x_{lat}$ , (ii) vessel distance to the receiving BS,  $d$ , (iii) RSSI at the BS, (iv) receiving (BS') and transmitting (vessel's) antenna heights,  $h_R$ ,  $h_T$ , and (v) vessel length,  $L$ . Specifically, some features are used

only for the building of the BS normality model ((i), (iii) and (v)), while the remaining ones ((ii) and (iv)) are exploited to build the single vessel normality model, as will be detailed later in the paper.

#### 4.2. BS normality model building strategies: averaged RSS Raster and one-class SVM

The features extracted from the training data set, represented by historical AIS messages collected by the BS under analysis, are a model for the normality scenario. The BS normality model  $\lambda_{BS}$  has been built by using the two following approaches: (i) the One-class SVM, and (ii) the Averaged RSS Raster (ARR).

##### 4.2.1. One-class SVM

The first approach can be framed in the context of classifications problem which, traditionally, try to solve the two or multi-class situation (Alpaydin, 2010; Murty, 2011). The goal of this well-known machine learning application is to distinguish test data between a number of classes, using training data.

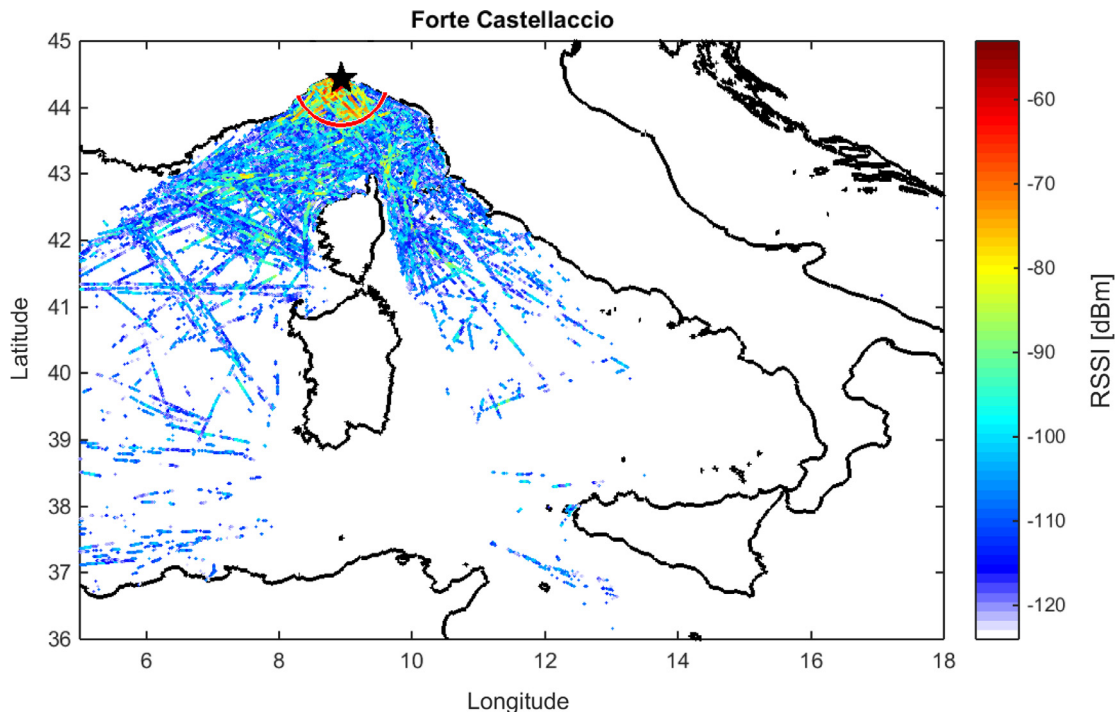


**Fig. 7.** Aggregate behaviour of the RSSI measurements collected by the BS located on Forte Castellaccio, Genoa, between July, 7 and July 15, 2016, highlighting the strong extension of radio coverage beyond the LOS distance. The red circle approximately defines the LOS distance, while BS can see vessels until around 900 km. (For interpretation of the references to colour in this figure legend, the reader is referred to the web version of this article.)

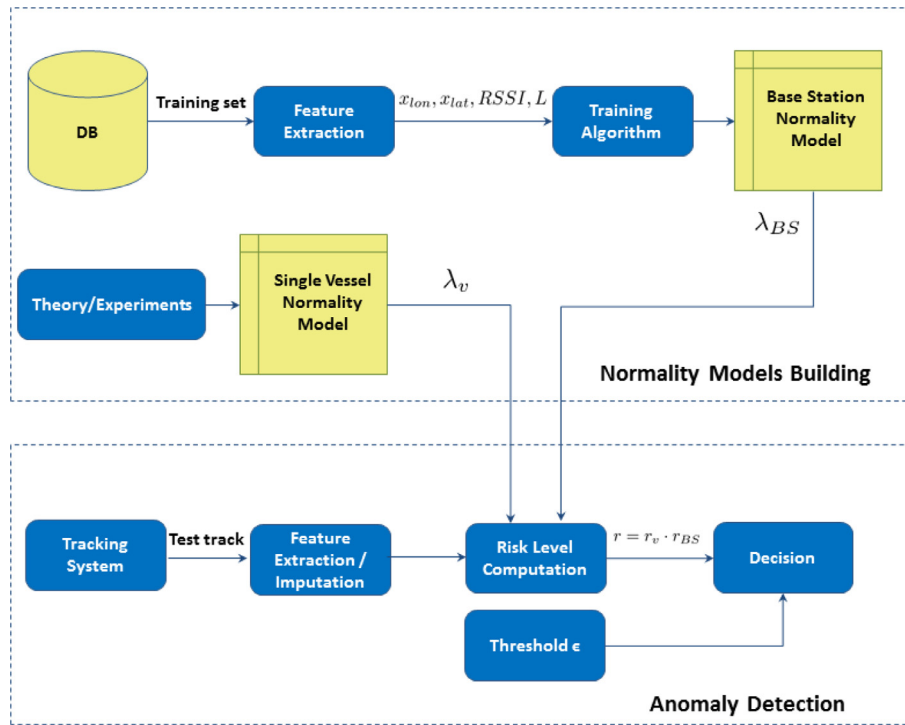


**Fig. 8.** Top: Block diagram of the normality model creation stage; Bottom: Block diagram of the anomaly detection stage.

Nevertheless, in many anomaly detection applications, only data of one class are available and the final objective is to state whether new data are alike or not like the training data. In these cases, training data from the only available class are used to determine a detection threshold that will partition the state space in two regions: one region corresponding to the hypothesis  $\mathcal{H}_0$  (normal behaviour), and the other one corresponding to the hypothesis

$\mathcal{H}_1$  (anomaly). In the classification literature similar problems have been referred to as one-class classification or *novelty detection* (Pimentel, Clifton, Clifton, & Tarassenko, 2014; Schölkopf & Smola, 2001). A methodology solving this problem, which gained much popularity in the last decades is the aforementioned One-class SVM (Schölkopf, Williamson, Smola, Shawe-Taylor, & Platt, 2000). Applications of the One-class SVM strategy to diverse

detection issues can be found in Ma and Perkins (2003), Li, Huang, Tian, and Xu (2003), Shawe-Taylor and Žličar (2015) and Erfani, Rajasegarar, Karunasekera, and Leckie (2016).

Let us first take a look at the classical two-class SVM problem (Murty, 2011), a supervised learning model. Typically, the SVM algorithm is given a set of training examples labelled as belonging to one of two classes, that is, a set  $\Omega = \{(\mathbf{z}_1, y_1), \dots, (\mathbf{z}_n, y_n)\}$  points, with  $\mathbf{z}_i \in \mathbb{R}^d$ , where  $\mathbf{z}_i$  is the  $i$ th input data point and  $y_i \in \{-1, +1\}$  is the  $i$ th output pattern, indicating the class membership. The SVM algorithm represents the training examples as points in space, mapped so that the examples of the separate categories are divided by a clear gap that is as wide as possible. New examples are then mapped into that same space and predicted to belong to one category or another, based on which side of the gap they fall on. A very interesting property of SVM is that it can create a non-linear decision boundary by projecting the data through a non-linear function  $\phi$  to a space with a higher dimension. This means that data points which cannot be separated by a straight line in their original space  $I$  are lifted to a feature space  $F$  where there can be a *straight* hyperplane that separates the data points of one class from an other. When that hyperplane would be projected back to the input space  $I$ , it would have the form of a non-linear curve. The function  $\mathbf{K}(\mathbf{x}, \mathbf{z}_i) = \phi(\mathbf{x})^T \phi(\mathbf{z}_i)$  is called *kernelfunction*. Popular choices for the kernel function are linear, polynomial, sigmoidal but mostly the Gaussian Radial Base Function (RBF), defined as:

$$\mathbf{K}(\mathbf{x}, \mathbf{z}_i) = \exp(-\gamma \|\mathbf{x} - \mathbf{z}_i\|^2), \quad (8)$$

where the parameter  $\gamma > 0$  sets the spread of the kernel.

The One-class SVM in Schölkopf et al. (2000) separates all the data points from the origin (in feature space  $F$ ) and maximizes the distance from this hyperplane to the origin. This results in a binary function which captures regions in the input space where the probability density of the data lives. Thus the function returns  $+1$  in a small region (capturing the training data points) and  $-1$  elsewhere. In this case, the following quadratic programming problem has to be solved:

$$\min_{\omega, \rho, \xi_i} \frac{1}{2} \|\omega\|^2 + \frac{1}{vn} \sum_{i=1}^n \xi_i - \rho \quad (9)$$

subject to

$$\begin{aligned} \omega \cdot \phi(\mathbf{z}_i) &\geq \rho - \xi_i, \quad i = 1, \dots, n \\ \xi_i &\geq 0. \end{aligned} \quad (10)$$

If  $\omega$  and  $\rho$  solve this problem, then the decision function  $f(\mathbf{z}_i) = \text{sign}((\omega \cdot \phi(\mathbf{z}_i)) - \rho)$  will be positive for most examples  $\mathbf{z}_i$  contained in the training set. In this formula it is the parameter  $v$  that characterizes the solution. In particular, (1) it sets an upper bound on the fraction of outliers (training examples regarded out-of-class) and, (2) it represents a lower bound on the number of training examples used as Support Vector. Due to the importance of this parameter, this approach is often referred to as  $v$ -SVM.

In the scenario under analysis in this paper, the final goal is to figure out whether missing AIS messages represent an anomalous situation or not. If we are able to reconstruct missing features and prove that the estimated values belongs to the normality class  $\mathcal{H}_0$ , it means that in normal conditions an AIS message should have been received and the dropout corresponds to an alerting situation. Then, in this first approach, an One-class SVM is trained by using latitude/longitude coordinates, RSSI information, and vessel length  $L$ , namely the vector  $[x_{lon}, x_{lat}, \text{RSSI}, L]$ , so that a normality model,  $\lambda_{BS}$  can be obtained, as described in Fig. 8. As previously discussed, the main degrees of freedom in this approach are the choice of the kernel function, together with its parameters, and the fraction of outliers in training set,  $v$ .

#### 4.2.2. ARR

With the regard to the other approach, the exploited features are again the vessel position coordinates in latitude/longitude, the vessel length  $L$ , and RSSI information of AIS training data set, combined in the vector  $[x_{lon}, x_{lat}, \text{RSSI}, L]$ . In this case, the BS normality model  $\lambda_{BS}$  is a geo-referenced *raster*. In geospatial analysis, a raster is a rectangular, regular grid that represents continuous data over geographical space. Cells are arranged in rows and columns and each holds a value. A raster is accompanied by metadata that indicate the resolution, extent and other properties. In this case,  $\lambda_{BS}$  represents a raster whose  $i$ th generic cell contains the median value,  $\bar{P}_i$ , of the RSSI measurements collected in that cell during a certain time interval. The idea of exploiting median values aims at discarding outliers. In addition, it is possible to normalize the median values of the RSSI with the respect to the extreme values measured for the BS and the time interval under analysis. This means that the raster will only contain values in the range  $[0, 1]$ . A cell will be characterized by a null value if there have been collected no measurements in the area related to that cell. The maximum value for a cell will be reached when the median value of the RSSIs received in that cell is the highest amongst the whole raster. The resolution of the raster will affect the capability of taking into account local phenomena: the more high is the resolution, the more local propagating effects will be contained in the normality model.

#### 4.3. Single vessel normality model

As described in Section 3, the AIS reception characteristics strongly depends on the electromagnetic properties of the BS under analysis. However, the propagation phenomena strongly changes among different vessels. Consequently, the decision procedure cannot ignore the behaviour of the single vessel. The single vessel normality model  $\lambda_v$ , as highlighted in Section 3.2, is a quasi-deterministic model made of the well-known FSL approximation when the distance between transmitter and receiver is less than the critical distance, and the ITU-R P.1546 for distances beyond the critical distance until the LOS range. Differently from the BS normality model, the single vessel normality baseline is not a data-driven model and the only features needed for the building of  $\lambda_v$  are the vessel's antenna height  $h_T$  and the height of the BS receiver,  $h_R$ . Indeed, by using these two features, the LOS range  $R$  and the critical distance  $d_c$  can be evaluated in a straightforward manner through the approximations in (1) and (5).

#### 4.4. Risk levels computation

The anomaly detection stage in the bottom panel of Fig. 8, applied on a set of vessel tracks,  $\{\mathbf{S}_i\}_{i=1}^N$ , goes through the following steps, summarized in Algorithm 1. All the vessel tracks, namely spatio-temporal trajectories containing both dynamic and static/voyage-related information about the vessels, are processed every  $\delta_T$  min in order to check for the occurrence of dropouts. Let us consider the algorithm behaviour for the  $i$ th vessel track at time  $t_k$ . First, if the track under consideration has available an AIS message at time  $t_k$ , there is no dropout. Otherwise, a dropout occurs at time  $t_k = t_d$ , and the track is pre-processed in order to extract the whole set of features required for the next steps. As described in Section 2, some features can be estimated through the tracking system (e.g.  $x_{lon}$ ,  $x_{lat}$ ,  $d_d$ ) by using one amongst the prediction algorithms developed in Mazzarella et al. (2013, 2015). The RSSI information is obtained through a NN imputation process, and the remaining features (e.g.  $L$ ,  $h_T$  and  $h_R$ ) are already available from previous AIS messages related to the vessel under analysis. After this process has been completed, the vector of the features extracted for the vessel under analysis represents the test sample

**Algorithm 1** AIS on/off anomaly detector.

---

**Require:**  $\lambda_v, \lambda_{BS}, \{\mathbf{S}_i\}_{i=1}^N, \epsilon, \delta_T, T$

- 1: **while**  $t_k < T$  **do**
- 2:    $k \leftarrow k + 1$
- 3:    $t_k \leftarrow t_{k-1} + \delta_T$
- 4:   // Iterate over all the vessel tracks
- 5:   **for**  $i = 1$  to  $N$  **do**
- 6:     // Check AIS message availability at time  $t_k$
- 7:      $[\mathbf{x}_{i,S}] \leftarrow \text{check\_dropout}(\mathbf{S}_i, t_k)$
- 8:     **if**  $\text{isempty}(\mathbf{x}_{i,S})$  **then**
- 9:       // There is a dropout
- 10:      // Feature extraction/imputation
- 11:       $[\mathbf{x}_{lon}, \mathbf{x}_{lat}, \text{RSSI}, L, d_c, d_d, R] \leftarrow \text{feature\_extraction}(\mathbf{S}_i, t_k)$
- 12:      // Single vessel risk level computation
- 13:       $r_v \leftarrow \text{single\_vessel\_risk}(\lambda_v, d_d, d_c, R)$
- 14:      // BS risk level computation
- 15:       $r_{BS} \leftarrow \text{BS\_risk}(\lambda_{BS}, \mathbf{x}_{lon}, \mathbf{x}_{lat}, \text{RSSI}, L)$
- 16:      // Joint risk level computation
- 17:       $r \leftarrow r_v \cdot r_{BS}$
- 18:      // Decision
- 19:      **if**  $r > \epsilon$  **then**
- 20:       // Dropout flagged as anomalous
- 21:        $an_{i,t_k} = 1$
- 22:      **else**
- 23:       // Dropout flagged as not anomalous
- 24:        $an_{i,t_k} = 0$
- 25:      **end if**
- 26:      **else**
- 27:       // The message is available, there is no anomaly
- 28:        $an_{i,t_k} = 0$
- 29:      **end if**
- 30:   **end for**
- 31:   // Return the list of dropout flags
- 32:   **return**  $\{an_{i,t_k}\}_{i=1}^N$
- 33: **end while**

---

that should be compared to the normality models,  $\lambda_v$  and  $\lambda_{BS}$  in order to compute two measures of the normality likelihood.

**4.4.1. Single vessel risk**

As described in [Section 3.2](#), the behaviour of the RSSI with the distance from the BS changes according to the critical distance  $d_c$  and LOS distance  $R$ . A first risk level,  $r_v$ , can be thus calculated by comparing the estimated dropout distance,  $d_d$ , to  $d_c$  and  $R$ . In particular, three possible scenarios can happen:

- $d_d \leq d_c \rightarrow \alpha \leq r_v < 1$ : The likelihood of an anomaly change ranges from high to medium according to the FSL approximation in [\(3\)](#), and a double check is fundamental to declare an intentional AIS switching off. In this case  $\alpha = \text{RSSI}|_{d=d_c} / \max(\text{RSSI})$
- $d_c < d_d \leq R \rightarrow \beta \leq r_v < \alpha$ : The likelihood of an anomaly is less than the previous interval, and the decreasing rate of the RSSI is faster than the previous distance interval. In this case, the risk level scales like the ITU model in [ITU \(2013\)](#) and  $\beta = \text{RSSI}|_{d=R} / \max(\text{RSSI})$ .
- $d_d > R \rightarrow 0 \leq r_v < \beta$ : The dropout occurs after the LOS, then the likelihood of an anomaly is very low, because the vessel starts going beyond the range of the radio coverage. However, this region should not be discarded as discussed in [Section 3](#), where it has been showed that several phenomena extends the AIS coverage beyond the LOS.

The risk level  $r_v$  calculated according to the methodology in the above represents then the likelihood of the test sample under the normality hypothesis  $\mathcal{H}_0$ . That means  $r_v \approx f(d_d; \mathcal{H}_0)$ .

**4.4.2. BS risk**

Given the normality model represented by the trained One-class SVM, a test feature vector  $[\mathbf{x}_{lon}, \mathbf{x}_{lat}, \text{RSSI}, L]$  feeds the aforementioned model in order to obtain a prediction on its label. If the output is the label  $-1$ , the test feature does not belong to the normality model and the dropout is not anomalous. Otherwise, the predicted label is  $+1$  and the observation belongs to the normality model. This means that the dropout is anomalous because an observation was expected. In this case, the risk level provided by the comparison between the test data and the BS-normality model,  $r_{BS}$ , is the score of the One-class SVM, conveniently transformed in a probabilistic output as suggested in [Platt \(1999\)](#).

Given the ARR raster, that represents the BS-based normality background, for a generic test feature vector  $[\mathbf{x}_{lon}, \mathbf{x}_{lat}, \text{RSSI}, L]$ , the first step is the evaluation of the corresponding cell in the raster, say  $j$ . Then, it is possible to approximate the likelihood of the test vector over the normality model as the value contained in the cell  $j$ . This value represents the risk level  $r_{BS}$  computed by the anomaly detector.

The risk level  $r_{BS}$  calculated according to one of the two methodologies in the above represents then the likelihood of the test sample under the normality hypothesis  $\mathcal{H}_0$ . That means  $r_{BS} \approx f(\mathbf{x}_{lon}, \mathbf{x}_{lat}, \text{RSSI}, L; \mathcal{H}_0)$ .

**4.5. Decision**

Given the feature vector  $[\mathbf{x}_{lon}, \mathbf{x}_{lat}, \text{RSSI}, L, d_d]$  extracted/imputed for the dropout at time  $t_k = t_d$ , an anomaly can be declared if the likelihood of the feature vector is greater than the threshold  $\epsilon$ . The likelihood can be approximated as:

$$\begin{aligned} f(\mathbf{x}_{lon}, \mathbf{x}_{lat}, \text{RSSI}, L, d_d; \mathcal{H}_0) &= f(d_d; \mathcal{H}_0) \cdot f(\mathbf{x}_{lon}, \mathbf{x}_{lat}, \text{RSSI}, L | d_d; \mathcal{H}_0) \\ &\approx f(d_d; \mathcal{H}_0) \cdot f(\mathbf{x}_{lon}, \mathbf{x}_{lat}, \text{RSSI}, L; \mathcal{H}_0) \\ &\approx r_v \cdot r_{BS}, \end{aligned} \quad (11)$$

by using the Bayes rule and the naive approximation involving the statistical independence between vector  $[\mathbf{x}_{lon}, \mathbf{x}_{lat}, \text{RSSI}, L]$  and  $d_d$ . A suboptimal decision rule can be thus based on the overall risk level defined as  $r = r_v \cdot r_{BS}$ . Then the risk level is compared against a threshold,  $\epsilon$ , in order to detect an intentional and anomalous dropout. In particular, if the obtained overall risk level exceeds the threshold, the dropout is marked as anomalous, i.e.  $an_{i,t_k} = 1$ , because, according to the normality model, an observation should be received at the dropout time, with a certain level of likelihood. The [Algorithm 1](#) produces as output a list of dropout flags, for the whole set of input vessel tracks.

[Fig. 9](#) shows an example of application of the proposed anomaly detection process for the receiving station located on Monte Capanne, on the Elba Island, and for a single vessel tracked during the first hours of May 1st, 2016. The vessel under analysis is a yacht leaving Elba Island, whose track together with the values of RSSI are represented in [Fig. 9\(a\)](#). Suppose that the proposed anomaly detector, in real-time operations, checks the availability of AIS messages every  $\delta_T = 15$  min. The black square in [Fig. 9\(a\)](#) represents the occurrence of the first dropout, at time  $t_d$ . According to the [Algorithm 1](#), the next step consists of reconstructing the missing information on vessel position and RSSI at time  $t_d$ . Vessel position estimation can be made by the tracking system in [Fig. 1](#), by exploiting one amongst the methodologies developed in [Mazzarella et al. \(2013, 2015\)](#). In this paper, for the sake of simplicity and since the focus is on the anomaly detector behaviour, a Constant Velocity Model (CVM) is adopted for the prediction (see [Mazzarella et al., 2013](#)). The black square of [Fig. 9\(a\)](#)

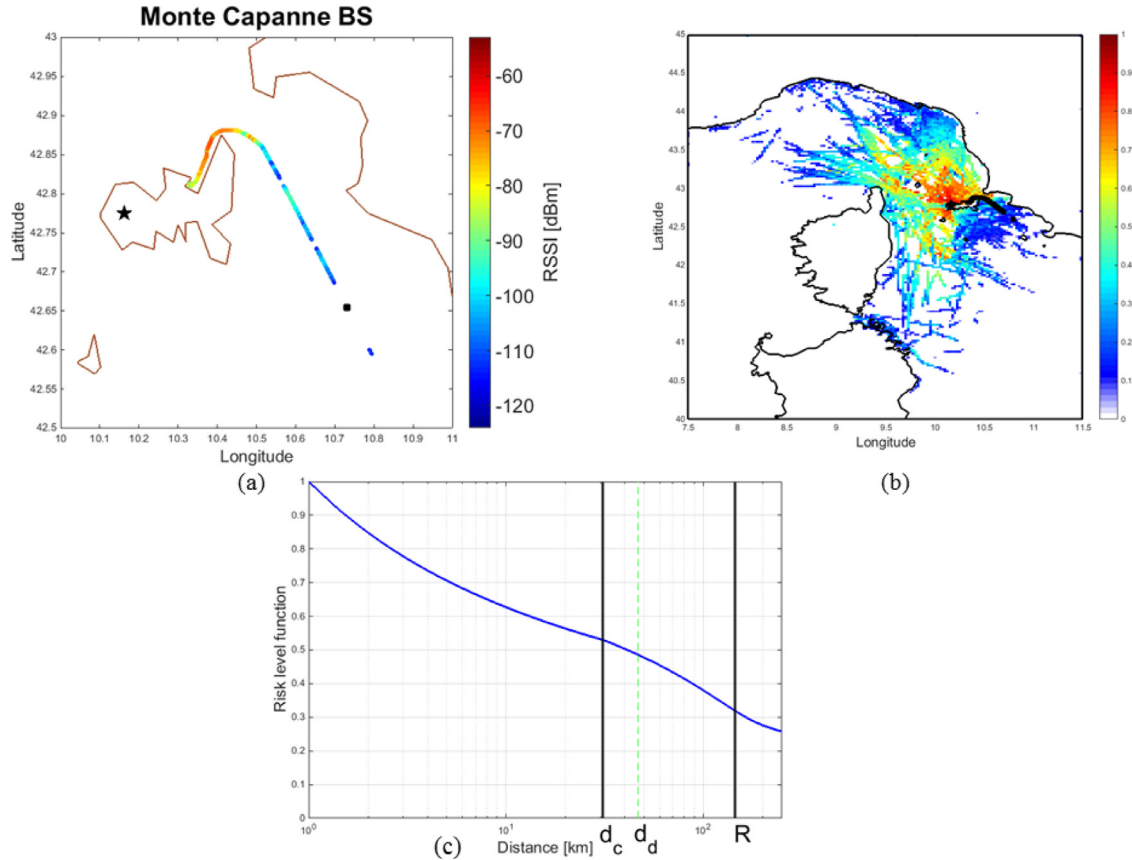


**Fig. 9.** Anomaly detector at work for the BS on Monte Capanne. (a) Vessel track under analysis, moving from the port of Livorno, during the time interval from midnight to noon of May 1 st, 2016. The colourbar refers to the RSSI measures at the BS. (b) Vessel track overlapped to the ARR raster describing, for every cell, the normalized median RSSI values. (c) Risk level function obtained as described in Section 4.3. Black lines represent the critical distance  $d_c$  and LOS range  $R$ , respectively, while the green line represents the dropout distance  $d_d$ , the distance from the BS where the first dropout occurs. (For interpretation of the references to colour in this figure legend, the reader is referred to the web version of this article.)

is such position prediction. The dropout distance from BS can be thus computed as the distance between the predicted position and the BS; in this case  $d_d = 46.5$  km. The imputation of RSSI values can follow one amongst the methodologies in Section 2. In this paper, the NN approach is adopted, where the imputed value is the RSSI received at the nearest point to the predicted one. The reconstructed feature vector  $[x_{lon}, x_{lat}, \text{RSSI}, L, d_d]$  is then used to compute the normality likelihood through the normality models  $\lambda_v$  and  $\lambda_{BS}$ . The single vessel normality model can be translated into the risk level function depicted in Fig. 9(c) as described in Section 4.3, where the critical distance and the LOS range for the vessel under investigation amount to  $d_c = 31$  km and  $R = 144$  km, respectively. The dropout distance is just beyond the critical distance and if we looked only at the single vessel behaviour, the dropout will be declared as anomalous with a risk level around 0.5. The BS normality model is depicted in Fig. 9(b) as a raster of normalized and averaged RSSI measurements and a cell resolution of 0.025 degrees obtained from vessel with length less than 75 m, being the vessel under analysis 50 m long. This normality model states that, for the reconstructed sample, we are in cell with a very low risk level. In particular, we get  $r_{BS} \approx 0.18$  and the dropout will be declared anomalous with a very low level of likelihood. This example shows how the joint use of both the normality vessel can help in decreasing the false alarm probability, as will be clear from the final performance of the detector given in the next Section.

## 5. Result analysis

The proposed methodology, described in Figs. 1 and 8, has been applied to real-world AIS data and the performance analysis is restricted to a single BS. In particular, we have considered the Pantelleria BS, whose aggregated behaviour, in terms of RSSI measurements, is represented in Fig. 6 for different vessel classes.

On the training side, we have used the full AIS data set received by the Pantelleria BS in the time interval between April 1 and April 10, 2016. Being the behaviour of AIS channel affected by the size of the vessels under analysis, we have partitioned the training data set in three categories: (i) vessels with  $L < 75$  m; (ii) vessels with  $75 \leq L < 150$  m; and (iii) vessels with  $L \geq 150$  m. Three models have been then trained for both methodologies presented in Section 4.2.

For the one-class SVM, the models have been built by using the LIBSVM toolbox in Chang and Lin (2011) with a Radial Basis Function (RBF) kernel and exploiting as training features the longitude/latitude vessel coordinates, the RSSI, and the vessel lengths  $L$ . The parameter  $\nu$  has been set to 0.05, while the spread RBF kernel has been set to 1. As for the training step of the ARR approach, three rasters have been built based on the AIS data related to the aforementioned time interval and vessel size classes. In particular, the AOI has been partitioned in cells of size  $0.025^\circ \times 0.025^\circ$ . Every cell is assigned the median value of the RSSI measurements falling in that cell, normalized with respect to extreme values, such that the resulting rasters contain values in the range [0, 1].

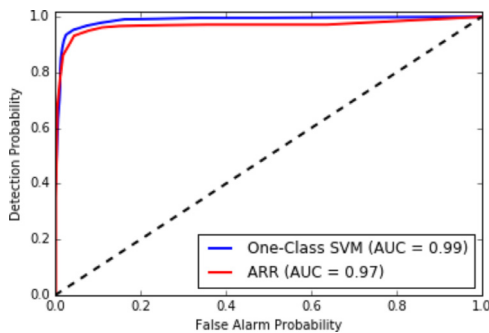


**Fig. 10.** Receiving Operating Characteristics (ROC) for the proposed algorithm with One-class SVM model (blue) and ARR normality model (red). The legend reports also the Area Under Curve (AUC) for each strategy. The black straight line is the ROC of a detector randomly guessing on the state of the nature. (For interpretation of the references to colour in this figure legend, the reader is referred to the web version of this article.)

On the test side, we have considered AIS data collected in a time interval non-intersecting with that used in the training step. In particular, we have analysed the AIS data set received during the whole day of June 1st, 2016. In order to provide results on the performance of the proposed methodology, it is necessary to evaluate the capabilities of the algorithm to detect anomalies and its robustness against false alarms. In the experiments conducted in this work, true and false anomalies have been generated as follows:

- *true* anomalies have been simulated by randomly removing from vessel tracks those observations with  $\text{RSSI} > -100 \text{ dBm}$ . These dropout events well represent scenarios where AIS vessel transponders have been switched-off.
- *false* anomalies have been generated, for each vessel track, by taking AIS messages not received from the BS under analysis but seen from a close BS (Monte Cammarata, Palermo, in this case). These messages represent false anomalies because they have been broadcast by transponders, but have not been received by the BS under analysis for other reasons than intentional AIS on-off switching.

The system performance has been evaluated in terms of detection probability,  $P_d$ , and false alarm probability  $P_f$ . Specifically, they are empirically computed from the detections achieved over the test set, as:

$$P_d = \frac{\text{no. of anomalous dropouts detected as abnormal}}{\text{no. of anomalous dropouts}}, \quad (12)$$

$$P_f = \frac{\text{no. of normal dropouts detected as abnormal}}{\text{no. of normal dropouts}}. \quad (13)$$

The Receiving Operating Characteristics (ROC) have been obtained varying the detection threshold between the minimum and the maximum value of the risk level returned by the test data. More in details, setting a threshold value lower than the minimum overall risk level, the system has null  $P_f$  and  $P_d$ . On the other extreme, instead, when the threshold is greater than the maximum risk level, both probabilities are 1 and each dropout is flagged as abnormal.

The ROC for the anomaly detection algorithm proposed in this paper are represented in Fig. 10, for both the BS-based normality model building approaches. The ROC in Fig. 10 have been obtained by running the anomaly detection algorithm on every track test collected during the whole day of June 1st with a dropout interval of 15 min. The false alarm and detection probabilities have been then averaged, for every threshold, over the full test data set. The

black straight line in Fig. 10 represents the ROC of a detector that randomly guesses the state of the nature (e.g.  $\mathcal{H}_0$  or  $\mathcal{H}_1$ ).

The performance of the detectors can be compared in terms of the ROC Areas Under Curve (AUC), whose values are reported in the legend of Fig. 10. The plots in Fig. 10 and the AUC values clearly highlight that the proposed algorithm with One-class SVM outperforms the one with ARR approach. In addition, the One-class SVM based algorithm is able to make the false alarm probability fall below 10% while keeping the detection probability above 90%.

## 6. Conclusions

In this paper, an anomaly detection methodology to identify intentional AIS On-Off transitions of vessel tracking data has been presented. Given that the AIS is a ship self-reporting system, the verification of the trustworthiness of AIS messages represent a key problem to exploit the full potential of this technology for a wide range of applications, spanning from knowledge discovery to anomaly detection on vessel movements. Several works dealing with the study of AIS message errors and falsification are available in literature. This paper focuses instead on the less-investigated issue of intentional AIS emission terminations, which could be aimed at engaging in illegal activities. The whole study leverages on the Received Signal Strength Indicator (RSSI), a feature available at the base stations and, up to the authors' knowledge, rarely exploited in the maritime domain applications.

The contribution of this paper is twofold. First, it has been demonstrated how the information about signal strength is crucial and how it has to be analysed in relation to parameters that are static with time (e.g. vessel and receiving station antenna heights), geographically variable (e.g. antenna pattern on receive, shadowing) and variable with time (e.g. atmospheric conditions). This analysis allowed for the building of two sound normality models (one based on single vessels behaviour and the other one for base stations) representing the baselines of the anomaly detector. Second, two approaches have been proposed to build the base station normality models, one based on the well-known One-Class Support Vector Machine, and the other one (the Averaged RSSI Raster) based on the geo-spatial distribution of RSSI historical measurements. The validity of the aforementioned approaches has been confirmed by the achieved results, and the suitability for real applications has been proven using a real-world AIS dataset. In particular, the One-class SVM algorithm can lead to significant performance in terms of detection probability and false alarm rates.

Differently from the other one state-of-the art method, the proposed algorithm has the capability to execute a detection for whatever time interval. Therefore, the system executes an on-line anomaly detection allowing for a real-time monitoring, as required by security and safety applications. In addition, the methodology introduced is scalable from one station to a network of receivers with overlapping fields of view. Future work shall consider also the possibility to detect anomalous transitions On-Off also beyond the line-of-sight by exploiting the knowledge of weather conditions at sea.

## References

- Alpaydin, E. (2010). *Introduction to machine learning* (2nd). The MIT Press.
- Angrisano, A., Gaglione, S., & Gioia, C. (2013). Performance assessment of aided global navigation satellite system for land navigation. *IET Radar, Sonar Navigation*, 7(6), 671–680.
- Baldazzi, M., Pasta, A., & Wilhoit, K. (2014). A security evaluation of ais automated identification system. In *Proceedings of the 30th annual computer security applications conference, ACSAC '14* (pp. 436–445). New York, NY, USA: ACM. doi:10.1145/2664243.2664257.
- Barclay, L. (Ed.), (2003). Propagation of radiowaves. Electromagnetic waves. Institution of Engineering and Technology.
- Bullington, K. (1947). Radio propagation at frequencies above 30 megacycles. *Proceedings of the IRE*, 35(10), 1122–1136. doi:10.1109/JRPROC.1947.232600.

- Chang, C.-C., & Lin, C.-J. (2011). Libsvm: A library for support vector machines. *ACM Transactions Intelligent Systems and Technology*, 2(3), 27:1–27:27. doi:10.1145/1961189.1961199.
- Erfani, S. M., Rajasegarar, S., Karunasekera, S., & Leckie, C. (2016). High-dimensional and large-scale anomaly detection using a linear one-class SVM with deep learning. *Pattern Recognition*, 58, 121–134.
- European Commission (2009). Strategic goals and recommendations for the EU's maritime transport policy until 2018, com(2009) 8 final.
- European Parliament (2002). Directive 2002/59/EC of the European Parliament and of the Council establishing a Community vessel traffic monitoring and information system, as amended by Directive 2009/17/EC and Commission Directive 2011/15/EU.
- Fox, J. (2008). *Applied regression analysis and generalized linear models*. SAGE Publications.
- Green, D., Fowler, C., Power, D., & Tunaley, J. K. E. (2011). VHF propagation study. *Contract Report, R-11-020-868*. Defense Research and Development Canada.
- Guerrero, M., Coraluppi, S., Carthel, C., & Willett, P. (2010). Analysis of AIS intermittency and vessel characterization using a hidden markov model. In K.-P. Fhnrich, & B. Franczyk (Eds.), *Gi Jahrestagung* (2): 176.
- Handayani, D. O. D., Sediono, W., & Shah, A. (2013). Anomaly detection in vessel tracking using support vector machines (SVMs). In *Proceedings of the 2013 international conference on advanced computer science applications and technologies, ACSAT '13* (pp. 213–217). Washington, DC, USA: IEEE Computer Society. doi:10.1109/ACSAT.2013.49.
- Harati-Mokhtari, A., Wall, A., Brooks, P., & Wang, J. (2007). Automatic identification system (AIS): Data reliability and human error implications. *Journal of Navigation*, 60(3), 373–389.
- Hruschka, E. R., Hruschka, E. R., & Ebecken, N. F. F. (2007). Bayesian networks for imputation in classification problems. *Journal of Intelligent Information Systems*, 29(3), 231–252.
- Iphar, C., Napoli, A., & Ray, C. (2015). Detection of false AIS messages for the improvement of maritime situational awareness. In *Oceans 2015 - mts/ieee washington* (pp. 1–7).
- ITU (2013). Method for point-to-area predictions for terrestrial services in the frequency range 30 MHz to 3000 MHz.
- Jiahua Chen, J. S. (2001). Jackknife variance estimation for nearest-neighbor imputation. *Journal of the American Statistical Association*, 96(453), 260–269.
- Katsilieris, F., Braca, P., & Coraluppi, S. (2013). Detection of malicious AIS position spoofing by exploiting radar information. In *Information fusion (fusion), 2013 16th international conference on* (pp. 1196–1203).
- Laxhammar, R., Falkman, G., & Sviestins, E. (2009). Anomaly detection in sea traffic - a comparison of the gaussian mixture model and the kernel density estimator. In *Information fusion, 2009. fusion '09. 12th international conference on* (pp. 756–763).
- Li, K.-L., Huang, H.-K., Tian, S.-F., & Xu, W. (2003). Improving one-class SVM for anomaly detection. In *Machine learning and cybernetics, 2003 international conference on*: 5 (pp. 3077–3081 Vol. 5). doi:10.1109/ICMLC.2003.1260106.
- Ma, J., & Perkins, S. (2003). Time-series novelty detection using one-class support vector machines. In *Neural networks, 2003. proceedings of the international joint conference on*: 3 (pp. 1741–1745 vol. 3). doi:10.1109/IJCNN.2003.1223670.
- Mazzarella, F., Alessandrini, A., Greidanus, H., Alvarez, M., Argentieri, P., Nappo, D., & Ziemia, L. (2013). Data fusion for wide-area maritime surveillance. In *Workshop on moving objects at sea, Brest, France* (pp. 1–4).
- Mazzarella, F., Arguedas, V. F., & Vespe, M. (2015). Knowledge-based vessel position prediction using historical AIS data. In *Sensor data fusion: Trends, solutions, applications (sdf)*, 2015 (pp. 1–6).
- Mazzarella, F., Vespe, M., Damalas, D., & Osio, G. (2014). Discovering vessel activities at sea using AIS data: Mapping of fishing footprints. In *Information fusion (fusion), 2014 17th international conference on* (pp. 1–7).
- Mazzarella, F., Vespe, M., Tarchi, D., Aulicino, G., & Vollero, A. (2016). AIS reception characterisation for AIS on/off anomaly detection. In *Information fusion (fusion), 2016 19th international conference on* (pp. 1–7).
- Murty, N. (2011). Pattern recognition : An algorithmic approach. *Undergraduate topics in computer science*. New York: Springer.
- Natale, F., Gibin, M., Alessandrini, A., Vespe, M., & Paulrud, A. (2015). Mapping fishing effort through AIS data. *PLoS ONE*, 10(6), 1–16.
- Norton, K. A. (1941). The calculation of ground-wave field intensity over a finitely conducting spherical earth. *Proceedings of the IRE*, 29(12), 623–639.
- Pallotta, G., Horn, S., Braca, P., & Bryan, K. (2014). Context-enhanced vessel prediction based on ornstein-uhlenbeck processes using historical AIS traffic patterns: Real-world experimental results. In *Information fusion (fusion), 2014 17th international conference on* (pp. 1–7).
- Pallotta, G., Vespe, M., & Bryan, K. (2013). Vessel pattern knowledge discovery from AIS data: A framework for anomaly detection and route prediction. *Entropy*, 15, 2218–2245.
- Papi, F., Tarchi, D., Vespe, M., Oliveri, F., Borghese, F., Aulicino, G., & Vollero, A. (2015). Radiolocation and tracking of automatic identification system signals for maritime situational awareness. *Radar, Sonar Navigation, IET*, 9(5), 568–580.
- Pimentel, M. A., Clifton, D. A., Clifton, L., & Tarassenko, L. (2014). A review of novelty detection. *Signal Processing*, 99, 215–249. <http://dx.doi.org/10.1016/j.sigpro.2013.12.026>.
- Platt, J. C. (1999). Probabilistic outputs for support vector machines and comparisons to regularized likelihood methods. In *Advances in large margin classifiers* (pp. 61–74). MIT Press.
- Rancourt, B. (1999). Estimation with nearest-neighbor imputation at statistics canada. In *Proceedings of the survey research methods section, american statistical association* (pp. 131–138).
- Ristic, B., La Scala, B., Morelande, M., & Gordon, N. (2008). Statistical analysis of motion patterns in AIS data: Anomaly detection and motion prediction. In *Information fusion, 2008 11th international conference on* (pp. 1–7).
- Schölkopf, B., & Smola, A. J. (2001). *Learning with Kernels: Support vector machines, regularization, optimization, and beyond*. Cambridge, MA, USA: MIT Press.
- Schölkopf, B., Williamson, R. C., Smola, A. J., Shawe-Taylor, J., & Platt, J. C. (2000). Support vector method for novelty detection. In S. A. Solla, T. K. Leen, & K. Müller (Eds.), *Advances in neural information processing systems 12* (pp. 582–588). MIT Press.
- Shawe-Taylor, J., & Žličar, B. (2015). In I. Morlini, T. Minerva, & M. Vichi (Eds.), *Novelty detection with one-class support vector machines* (pp. 231–257). Cham: Springer International Publishing. [http://dx.doi.org/10.1007/978-3-319-17377-1\\_24](http://dx.doi.org/10.1007/978-3-319-17377-1_24).
- SOLAS (2000). Safety of life at sea convention chapter v, regulation 19.
- Vespe, M., Gibin, M., Alessandrini, A., Natale, F., Mazzarella, F., & Osio, G. C. (2016). Mapping EU fishing activities using ship tracking data. *Journal of Maps*, 12(sup1), 520–525. doi:10.1080/17445647.2016.1195299.
- Yang, K., Ekman, T., Rste, T., & Bekkadal, F. (2011). A quasi-deterministic path loss propagation model for the open sea environment. In *Wireless personal multimedia communications (wpmc), 2011 14th international symposium on* (pp. 1–5).
- Yang, K., Molisch, A. F., Ekman, T., & Roste, T. (2013). A deterministic round earth loss model for open-sea radio propagation. In *Vehicular technology conference (vtc spring), 2013 ieee 77th* (pp. 1–5).